JACS
JOURNAL OF THE AMERICAN CHEMICAL SOCIETY

Article

pubs.acs.org/JACS

New Insights into Single-Molecule Junctions Using a Robust, Unsupervised Approach to Data Collection and Analysis

Michael S. Inkpen,*[,†] Mario Lemmer,[†] Nathan Fitzpatrick,[†] David C. Milan,[‡] Richard J. Nichols,[‡] Nicholas J. Long,*[,†] and Tim Albrecht*[,†]

[†]Department of Chemistry, Imperial College London, London SW7 2AZ, U.K.

[‡]Department of Chemistry, University of Liverpool, Liverpool L69 7ZD, U.K.

Supporting Information

ABSTRACT: We have applied a new, robust and unsupervised approach to data collection, sorting and analysis that provides fresh insights into the nature of single-molecule junctions. Automation of tunneling current-distance ($I(s)$) spectroscopy facilitates the collection of very large data sets (up to 100 000 traces for a single experiment), enabling comprehensive statistical interrogations with respect to underlying tunneling characteristics, noise and junction formation probability (JFP). We frequently observe unusual low-to-high through-molecule conductance features with increasing electrode separation, in addition to numerous other "plateau" shapes, which may be related to changes in interfacial or molecular bridge structure. Furthermore, for the first time we use the JFP to characterize the homogeneity of functionalized surfaces at the nanoscale.

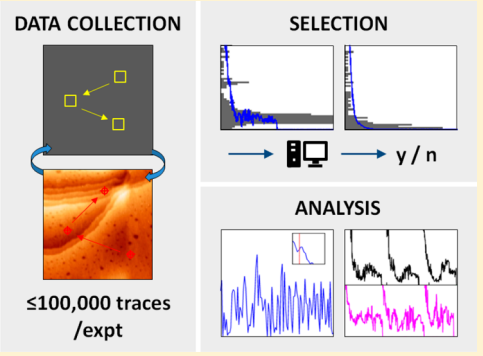

INTRODUCTION

Despite significant advances, the reliability and reproducibility of single-molecule conductance measurements remains a significant challenge.[1−8] Since Xu and Tao reported their scanning tunneling microscopy in situ break-junction (STM BJ) technique in 2003,[1] it has been adopted by numerous groups as a means to rapidly obtain hundreds or thousands of single-molecule conductance-distance measurements.[5,9−12] These are then typically analyzed using statistical methods—for example, 1D (conductance-count) or 2D (conductance-distance-count) histograms—to obtain the most probable molecular junction characteristics (conductance, plateau length, etc.). In contrast, compiling data sets of comparable sizes has proven difficult with complementary "conductance plateau" techniques such as the STM current-distance ($I(s)$) approach (also called the $I(z)$ method in some literature).[13−16] Here, experimental automation is less straightforward than in most BJ studies, for example, due to intermittent tip contamination (by "contamination" we mean here, for instance, accumulation of analyte on the tip during sustained molecular junction-making/breaking cycles). Additional difficulties are faced when processing the data, as the low junction formation probabilities which are often observed (JFPs, the number of measurements containing molecular features vs number of total measurements) pose challenges for the interpretation of all-data point analyses (where "low" ≈ <20%, "high" ≈ >40%). Motivated by a variety of prospective studies to which the $I(s)$ technique is particularly well-suited (described later), in this work we demonstrate a new methodology that significantly increases its utility (Figure 1). For example, by preserving the entire information content of a data set in addition to sorting single-molecule events objectively, it takes the middle-ground between the opposing philosophies of all data point versus selected data point analyses, thus enabling new experimental and statistical studies, as we show below. Second, the open availability of the sorting criteria facilitates a critical assessment of the analysis results (also between different research groups, for example) and contributes to the standardization of data analysis tools in this increasingly mature field of research. Third, it enables an unbiased view on the data as a whole or perhaps on emerging subpopulations, and on surface properties that are easily missed by hand selection or all-data point plots.

The differences between the STM BJ and $I(s)$ techniques can be attributed to the nature of tip−substrate interaction during measurements. Whereas the BJ approach involves the repeated formation and breaking of tip−substrate metal−metal contacts, the $I(s)$ method instead positions the tip a short distance from the substrate surface prior to tip withdrawal, and so the electrodes never meet. One important consequence of this is that the BJ method inevitably scrambles ordered surface-bound molecular layers (for example, forming nanofilaments[17]), whereas $I(s)$ approaches better preserve the underlying surface structure. The frequent renewing of electrode surfaces also allows BJ experiments to be conducted in dilute analyte solutions (typically 0.1−1 mM).[1,3,4] Here, the observation of high JFPs may be attributed to the rapid formation of molecular junctions upon breaking the metal−metal contacts. It is notable in this context that significantly reduced JFPs are observed in BJ experiments when only monolayer/submonolayer quantities of

Received: June 2, 2015
Published: July 16, 2015

DOI: 10.1021/jacs.5b05693
J. Am. Chem. Soc. 2015, 137, 9971−9981

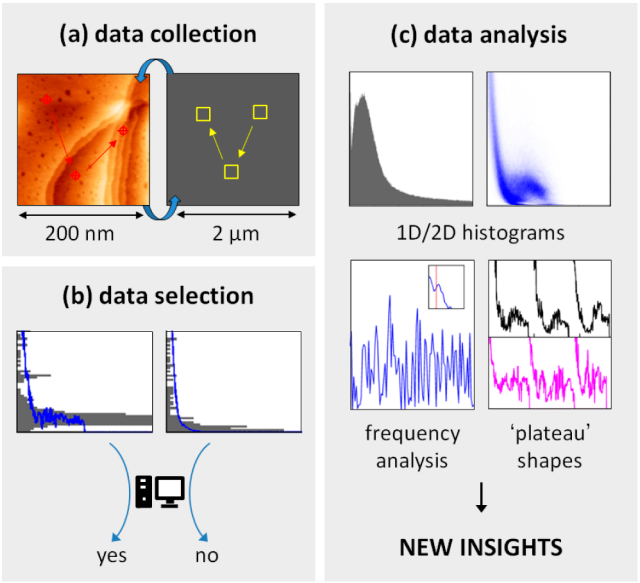

Figure 1. An overview of the new experimental and data analysis methodology described in this work: (a) STM tips collect $I(s)$ data at randomly chosen positions on a 200 nm^2 area, prior to repeating the process at other randomly selected 200 nm^2 locations on the substrate surface; (b) $I(s)$ traces are sorted using an objective algorithm; (c) sorted and unsorted data is analyzed using known and novel techniques.

analyte molecules are present.[18] In comparison, the $I(s)$ technique is normally used to probe prefunctionalized, low coverage surfaces in liquid,[19−21] air,[22] or vacuum.[23] Though this serves to minimize tip "contamination" and favor single-molecule junction formation,[24] it also naturally reduces the frequency at which analyte molecules are trapped between electrodes.

In any experiment where low JFPs prevail, the application of some form of data sorting/selection becomes extremely useful for improving the signal-to-noise ratio (and also to extract more detailed information). Such processes aim to identify traces comprising features relating to through-molecule conductance, ultimately eliminating featureless and/or "noisy" measurements from the data set (for example, those impacted by extrinsic vibrational/electrical effects). It should be stressed however that this is a remarkably nontrivial exercise, first requiring consideration of what comprises a molecular feature? In some reports, this intrinsic measurement ambiguity has been reduced using new experimental approaches which aid the assignment of data to "through-space" or "through-molecule" information (in addition to expanding the toolbox of available probe methods and enhancing the information content). Key examples include: (i) distance-modulation assisted BJ methods;[25,26] (ii) measurement of $I-V$ curves "midplateau" (accepting curves with comparable before and after conductance values);[27] (iii) "wiring" single-molecules between C_{60} termini (addressing relatively large end-groups rather than the molecule directly);[28] or (iv) employing "fluctuational statistics" (taking conductance measurements of highly stable molecular junctions over several days).[29] For most studies, however, this ambiguity cannot be resolved using the experimental method alone, whereby data sorting approaches such as hand-selection, "background" subtraction,[30] trace differentiation,[31] or multistep algorithms (above-threshold current detection and/or trace fitting)[2,18] become necessary. These methods are based on the appearance of data in the presence of analyte molecules, compared to its appearance in their absence. While all appear successful to varying degrees, to date we note there is no widely accepted technique.

Following the discussion above, we considered that a great number of intriguing research questions might be addressed if only the $I(s)$ technique's automation and sorting problems could be resolved. Its broad use in air on prefunctionalized substrates (in addition to its application in solutions and electrolytes[13]) suggests that it may easily transition to the interrogation of single-molecule thermoelectric effects.[32−35] In such studies, measurements outside of solution are necessary to maintain tip−surface temperature differentials. Furthermore, given that the tip and substrate materials do not make physical contact, the method is ideal for studies of surface-orientated asymmetrical molecules (probing single-molecule rectification[36−38]), on-surface (in situ) synthesized/modified components,[39,40] or experiments involving heterogeneous electrodes.[41,42] In a first step toward pursuits along these lines, herein we report an automated $I(s)$ data collection methodology (capable of recording 10 000 $I(s)$ measurements in ∼8 h) and a novel, mathematically rigorous data sorting algorithm which makes no assumptions about plateau shape (processing 10 000 $I(s)$ measurements in ∼2 h). With our approach, the number of measurements per experiment can be increased by 2 orders of magnitude compared to previous studies[5,13,15,19−21,24] using this method. This greatly expands the utility and accuracy of the $I(s)$ method as a tool for single-molecular studies. Furthermore, in our proof-of-concept experiments with 1,8-octanedithiol (**1,8-ODT**), we have observed frequent and unusual plateau "shapes" which may be related to changes in molecular junction structure upon elongation. Despite multiple studies with this analyte, such features appear to have previously drawn little comment. Through application of our plateau-detection algorithm to data sets comprising all data measured during experiments, we are also able to objectively interrogate JFP as a function of tip−substrate position for the first time. Such analyses offer new insights into the homogeneity of functionalized surfaces at the nanoscale.

RESULTS AND DISCUSSION

Automated Data Collection. Experimental parameters (including file names, number of experiments, bias voltage [V_{bias}], set point current [I_0], number of traces to measure, etc.) were set in a Microsoft Excel spreadsheet. These were imported as variables by a macro (written and played with Macro Scheduler) for input into commercial STM software (PicoView) as required (see STM Setup for more information). To check the stability of the STM tip−substrate contact, the tip was approached to a relatively low I_0 (for example, 0.5 nA) and the substrate briefly imaged. If the contact proved suitable (see STM Tip Preparation), the macro was subsequently played. Reproducibility of experimental results was aided by running the STM for ∼2 h before data was saved for analysis−ensuring thermal and mechanical equilibrium.

Automated $I(s)$ experiments were conducted as follows. A random 200 × 200 nm section of the surface was imaged, and the tip moved to a random $x-y$ coordinate within this area. By increasing I_0, the tip−substrate distance (s_0) was adjusted to a distance less than the calculated length of the analyte (facilitating tip binding to surface bound molecules). At this position, servo gain settings were reduced to help decouple latent tip movements from $I(s)$ traces after the servo controls

DOI: 10.1021/jacs.5b05693
J. Am. Chem. Soc. 2015, 137, 9971−9981

were disengaged. $I(s)$ traces were then measured using the in-built "spectroscopy" feature of the PicoView software. Here, with the servo controls automatically disengaged during measurements, the current was recorded (50 data points/Å) as the tip was withdrawn from s_0 to a distance greater than the length of the analyte (here 4 nm/0.48 s). After collecting 50−100 $I(s)$ traces at the first tip position, the same number were obtained at a further 4−9 randomly chosen x−y coordinates in the original 200 × 200 nm imaged area. A new imaging location was then randomly chosen, and the above steps repeated until the specified number of $I(s)$ traces for that experiment had been obtained (2000−100 000). At this point the next experiment was started (for example, using a different V_{bias}−I_0 combination), and the macro continued as before until all experiments were complete. By indiscriminately moving the tip to a large number of different locations, we aimed to sample as wide an area on the substrate surface as possible (noting that drift likely increases the actual number of sampled locations). This serves to average possible variations in $I(s)$ measurements relating to local changes in surface roughness or contamination.

In experiments with **1,8-ODT**, we occasionally observed consecutive series of $I(s)$ traces which were significant different from typical measurements. As these deviations were not seen with clean Au substrates, we attributed them to intermittent tip functionalization with surface-bound molecules. Two distinct tip-states could be identified: (i) "contamination", an inability to measure smooth $I(s)$ traces with a fast exponential decay (recording instead noisy traces with a slow decay; SI, Figure S1); and (ii) "passivation", a subtle but distinct reduction in experimental noise, with a striking decrease in JFP (SI, Figure S2). In both cases, reduced image quality was also observed (SI, Figure S3-left). Fortunately, it proved possible to expedite a return to normal behavior by either briefly increasing the servo I gain to 100% (inducing a rapid oscillation in the z-direction we call a "tip shake"), or by applying a "voltage pulse" between the tip and sample (9 V bias for 0.1 ms) (SI, Figure S2 and S3). The latter is known to result in transfer of atoms from tip to substrate (via field evaporation or as a result of large electrostatic forces).[43−45] Critical to improving the reproducibility of our results, we implemented these tip cleaning procedures as required using subroutines triggered using image recognition (Figure S1). A tip shake was systematically applied after detection of 5 consecutive traces with slow exponential decay, a voltage pulse after 15 consecutive traces, and the tip was moved to new x−y coordinates after 30 consecutive traces. To mitigate against reductions in JFPs due to "contamination" effects, we pre-empted tip passivation by systematically applying a voltage pulse before moving the tip to each new location or imaging area.

With such macro-control it proved possible to run $I(s)$ experiments unattended. However, we considered it prudent to intermittently check that the system was running smoothly, either in person, or using remote access software such as TeamViewer (Göppingen, Germany). Conveniently, it also proved possible to interface with the STM when "away-from-keyboard", using desktop-to-mobile instant messaging services such as Google Hangouts. Image recognition of (and responses to) specific commands were readily programmed. These included: "Pause" (pausing the macro midexperiment to allow access to the computer), "Next" (sending the STM tip to a new scan area) and "End" (terminating the experiment and withdrawing the STM tip to a safe distance). While in principle we were able to collect data automatically for indefinite time periods, most $I(s)$ measurements reported here were obtained ≤1 day after preparing samples (except for the 100 000 series, which was measured over 3 days).

Data Sorting Methodology. *Analysis of Model Data Sets.* We created several data sets comprising model $I(s)$ traces (SI, Figure S4), to test selection algorithms and explore in general how the JFP might impact our approach to data analysis. With these we simulated the effects of experimental noise, plateau length and plateau current distribution (SI, Figures S5−S7). Perhaps unsurprisingly, it was found that with increasing noise, decreasing plateau length, and broader distribution of current values, higher JFPs were necessary to resolve peaks with a reasonable signal-to-noise ratio. Applying conditions typical of experimental data, we determined that JFPs ≥20% might be necessary to successfully conduct all-data point analyses (SI, Figure S8). Given that previous applications of the $I(s)$ method had reported JFPs = 5−20%, it seemed likely that some form of data sorting would be required to improve the signal-to-noise ratio in our experiments. We set out to develop an objective algorithm to achieve this goal, to ensure our selection criteria would be consistent across each data set analyzed and also repeatable by others. (Our approach ultimately proved highly effective when applied to the aforementioned model data sets [SI, Figure S9], and is described in full in the next section.)

Analysis of Experimental Data Sets. Objectively sorting experimentally measured $I(s)$ traces is a nontrivial two-part problem. First the traces containing plateau-features (Figure 2b) must be separated from clean exponential curves (Figure 2a). Second, a distinction must be made between traces containing plateau-features and features relating to experimental noise (Figure 2c). Methods are demonstrated throughout this section using real data sets comprising 10 000 $I(s)$ measurements of a **1,8-ODT**-coated Au substrate (**1,8-ODT** 10 000 series) and 10 000 $I(s)$ measurements of a pure Au substrate (**blank** 10 000 series) (for both, V_{bias} = 0.3 V, I_0 = 20 nA).

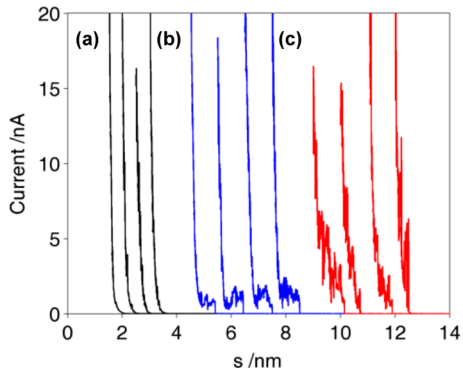

Figure 2. Representative $I(s)$ traces from a **1,8-ODT**-coated Au substrate (V_{bias} = 0.3 V, I_0 = 20 nA): (a) low-noise, fast exponential decays; (b) low-noise, fast exponential decays interrupted by "plateau" features (indicative of through-molecule current); (c) noisy, often slowly decaying exponential traces (displaced along the x-axis for clarity).

Identifying "Plateaus". We took inspiration from the widely used method for obtaining the most probable conductance value(s) of a molecular junction, plotting all $I(s)$ traces into a single 1D conductance-count histogram.[1] In such analyses, plateau features typically "add up" to give peaks. We reasoned

DOI: 10.1021/jacs.5b05693
J. Am. Chem. Soc. 2015, 137, 9971−9981

that similar "peaks" must also be recognizable in histograms of individual $I(s)$ traces, readily identifiable by a bin (or bins) exhibiting a higher count than those adjacent. Indeed this proved to be the case: a representative single-trace histogram with overlaid plateau-containing $I(s)$ trace is shown in Figure 3a. An analogous figure for a featureless $I(s)$ trace is shown in Figure 3b. Many more examples of this type can be found in the SI (Figure S10–S12).

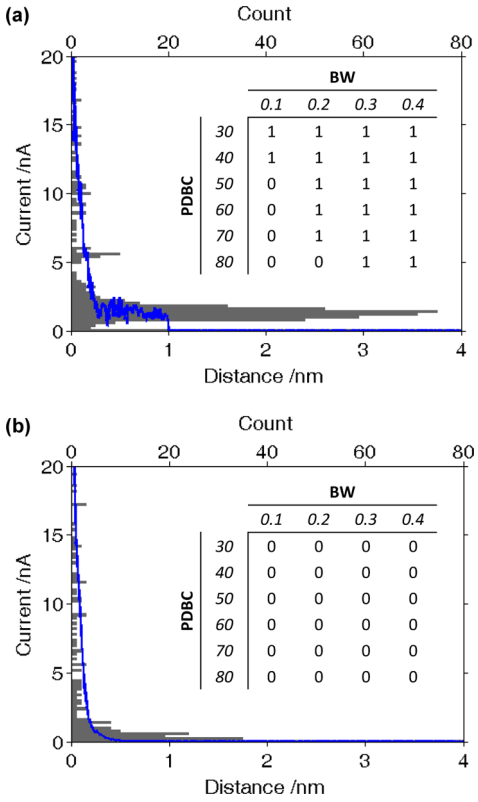

Figure 3. Single-trace histograms (BW = 0.2 nA) comprising overlaid individual $I(s)$ traces, (a) with and (b) without plateau features. Inset tables: sorting parameters that identify traces as containing (= 1) or not containing (= 0) a plateau.

We constructed a sorting algorithm which rapidly prepares and interrogates single-trace histograms for all $I(s)$ measurements. It identifies traces as containing plateaus if peaks in the single-trace histogram are detected which comprise bin counts higher than a preset value. (The high count "zero current" bin is accounted for in such analyses by accepting it must form the first "peak" from zero in every histogram. Only subsequent peaks are considered as resulting from possible plateaus.) This "plateau-determining bin count" (PDBC), in addition to the single-trace histogram bin width (BW), defines the sensitivity of the selection process. Unless otherwise stated we used a high sensitivity, employing BW and PDBC values that, even in control experiments on pure Au substrates, identified a number of $I(s)$ traces as containing "plateaus". While this approach may slightly reduce the signal-to-noise ratio by adding background data points, it errs on the side of caution by selecting the greatest number of molecular events possible (adding plateau data points). We note that it is also possible to determine an appropriate sensitivity experimentally, which in some cases can prove desirable (see below).

It was recognized that small BWs would favor the selection of low-noise, "flat" and well-defined plateaus, whereas large BWs would permit the selection of noisier, "slanted" and so perhaps poorly defined "plateaus". Important also, the smallest BW chosen dictates the minimum plateau current that can be detected. This is approximately twice the BW; the bin capturing data points from the plateau (the "peak" in the single-trace histogram) must be preceded by the "zero-current" bin (the 0 to 1×BW bin) and at least one bin of lower count (for example, the 1×BW to 2×BW bin). After binning, the PDBC must be appropriately adjusted (larger BW will capture more data points/bin, and vice versa). With low PDBCs any small deviations from the exponential decay may be considered a plateau, including artifacts arising from instrumental noise (as noted above). For higher PDBCs, only more significant deviations from the exponential decay will be identified (selecting longer plateaus). It can be seen that PDBCs between 30 and 80 would identify the unambiguous peak in Figure 3a (inset table), while ignoring smaller "peaks" in the histogram of Figure 3b.

Perhaps unsurprisingly, it ultimately proved unsuitable to use just a single parameter set (only one BW and one PDBC) to identify plateaus in a given data set. In this case the sorting algorithm becomes biased toward the selection of only one class of plateau (perhaps rejecting significant numbers of plateaus below the minimum detectable current level, or selecting only plateaus of similar shape or length). Indeed, variations in the most probable junction current can be observed with changing sorting parameters (SI, Figure S13–14). The situation is significantly improved if plateaus are selected across a wide range of parameter sets (we used BWs: 0.1–0.4 nS; PDBCs: 30–140). Any trace identified by any sorting parameter set as containing a "plateau" is accordingly added to a single list. Such an approach makes no assumptions about the shape, length or position of a through-molecule conductance feature, other than this must deviate from a simple exponential decay curve. The latter is observed almost exclusively for $I(s)$ measurements in the absence of surface-bound analyte molecules.

Reducing the Impact of "Contamination"/Noise. Using the above unsupervised approach to identify plateaus, $I(s)$ traces comprising noise features are also readily selected. While in some experiments these represent only a small minority of measured traces, in others they can prove a significant contribution to the total data set. Given that these artifacts are generated through intermittent tip/substrate-"contamination" or from extrinsic vibrational/electrical effects (even in the absence of surface-bound analyte), they are not representative of through-molecule conductance events. We consider it useful to have clear criteria by which they can be identified, and desirable to establish tools to remove them objectively so as to minimize experimental error.

It is possible to identify two properties associated with individual $I(s)$ traces that help achieve this goal: (i) a "noise factor" (NF); and (ii) an "exponential factor" (EF). The NF is calculated by taking the summed difference in current between successive data points eq 1. Small NFs are found for smooth, low-noise traces, and vice versa.

$$\mathrm{NF} = \sum_{i=2} \sqrt{(x_i - x_{i-1})^2} \tag{1}$$

The EF (essentially the tunneling decay constant), is obtained for each $I(s)$ trace by fitting it with an exponential

DOI: 10.1021/jacs.5b05693
J. Am. Chem. Soc. 2015, 137, 9971–9981

eq 2. To achieve good fits for traces containing plateau features, it is necessary to first remove data points associated with the latter. This was achieved using an unsupervised subroutine as part of our sorting algorithm (SI, Figure S15). The EF is particularly useful for identifying atypical traces, as slow decays are characteristic of tip or surface "contamination" (SI, Figure S1). As observed here and elsewhere,[46] faster decays can be achieved by applying cleaning procedures. In good agreement with our observations (Figure 4b), tunneling decay constants of

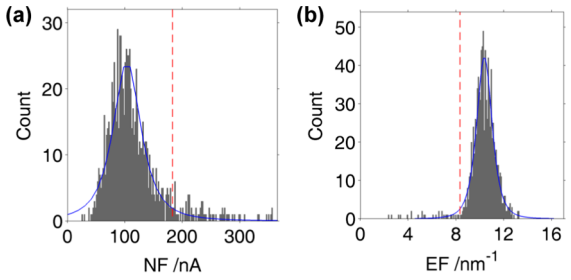

Figure 4. NF (a) and EF (b) histograms (gray bars) for a typical "low-noise" $I(s)$ experiment (sorting parameters: BW = 0.1 nA; PDBC = 40). The blue line shows the t-location scale distribution fit, with the red dotted line indicating $3\sigma_s$ cutoff values.

~1 Å^{-1} are typically observed for alkanethiol monolayers.[47−49] Many examples of $I(s)$ traces demonstrating their associated NFs and EFs (plus fits) are included in the SI (Figure S15 and S16).

$$I = ae^{(-\mathrm{EF}\times\mathrm{distance})} \quad (2)$$

For every group of "plateau-containing traces" identified by a given sorting parameter set (for example, BW = 0.1 nA, PDBC = 40), we compile all NF and EF values into histograms. While such histograms from typical "low-noise" experiments appear normally distributed for the most part, they exhibit heavier tails as a result of intermittent tip-functionalization or random experimental noise events (Figure 4). Accordingly, they are best fit with a t-location scale distribution, "useful for modeling data distributions with heavier tails (more prone to outliers) than the normal distribution".[50−53] In this context, the variance = $\sigma_s^2\nu/(\nu-2)$, where σ_s = scale parameter, ν = shape parameter. More examples of these noise histograms can be found in the SI (Figure S17 and S18). In excessively noisy/problematic experiments, bimodal distributions (or sometimes no clear distribution to fit) may be observed (SI, Figure S19).

In the first instance, noise analysis may simply be applied as a tool to determine the success or otherwise of an automated, unattended experiment (for example, checking that the STM tip has not degraded over time). This broadly eliminates the necessity to observe each and every individual $I(s)$ trace directly. In our analysis, however, traces with highly unusual noise properties (with NF = mean + $3\sigma_s$, and/or EF = mean − $3\sigma_s$) for each sorting parameter set were removed from the data set as outliers. If histograms were not easily fit with a distribution, no traces were excluded for that sorting parameter set. It is notable that some traces, while excluded according to the above criteria for one sorting parameter set, ultimately make the final list of plateau-containing traces after selection by alternative sorting parameters (SI, Figure S16).

With this approach we correct selection errors introduced by our plateau-identification mechanism, and demonstrate further how signal-to-noise ratios can be improved through objective analyses of complete data sets. However, the impact of the above noise analysis may prove ultimately insignificant with good data. For the **1,8-ODT** 10 000 series, only 8.4% of selected traces (2.6% of the total data set) were excluded for exhibiting unusual noise characteristics. A comparable number (1.8% of the total data set) were excluded from selected traces of the **blank** 10 000 series by applying the same analysis.

Conductance Measurements of 1,8-ODT. *Initial Studies: 10 000 I(s) Traces/Experiment.* Application of our sorting algorithm to the **1,8-ODT** 10 000 series selected 29% traces as containing plateaus, compared to 9% for the **blank** 10 000 series (V_{bias} = 0.3 V, I_0 = 20 nA). Figure 5 and 6 show 1D and

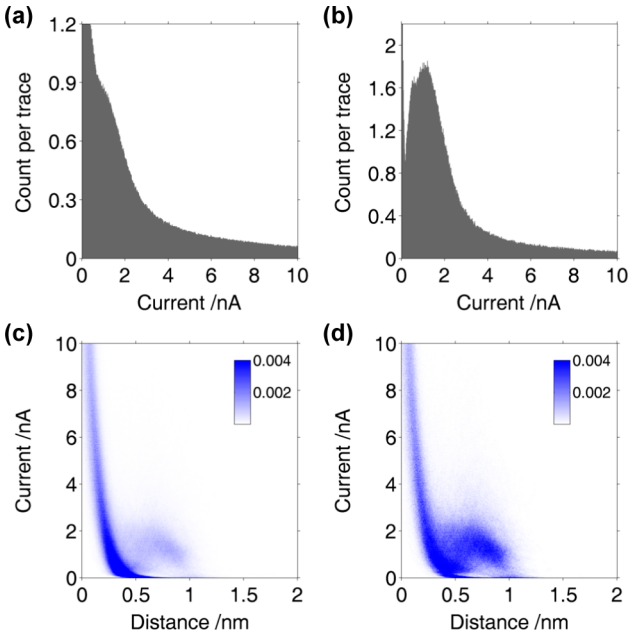

Figure 5. Top: Normalized 1D (a) all data point (10 000 traces) and (b) algorithm-selected (2859 traces) current-count histograms for the **1,8-ODT** 10 000 series (V_{bias} = 0.3 V, I_0 = 20 nA; 0.012 nA/bin). Bottom: Normalized 2D (c) all data point and (d) algorithm-selected current-distance-count histograms from the same data set (0.01 nA × 0.002 nm/bin).

2D histograms plotted before and after data selection for **1,8-ODT** and **blank** experiments, respectively. While faint features can be seen in the all-data point analyses, their clarity is greatly enhanced after processing. Testament to the objectivity of this sorting process, the character of the features (approximate position of most-probable current peak, apparent sine shape of plateau), also appears unchanged. An analogous result is obtained when plotting 1D and 2D histograms for the same data sets on a log-current scale (SI, Figure S20 and S21).

Attempts to fit the peak in Figure 5b (and analogous histograms from subsequent data sets) were not straightforward (SI, Figure S22, discussed in more detail below). However, reasonable representations of the distribution and peak value could be obtained in most cases using fits comprising a single Gaussian, providing a most probable conductance value of 3.83 nS (4.94×10^{-5} G_0; with a HWHM based on Gaussian fitting = 3.02 nS *or* 3.89×10^{-5} G_0). This is in good agreement with all subsequent experiments in this work, and the conductance obtained by numerous other groups using different methods (~5×10^{-5} G_0).[5,11,18,25,30,54−57] Within the proposed conductance group series for alkanedithiols (low/A, medium/

DOI: 10.1021/jacs.5b05693
J. Am. Chem. Soc. 2015, 137, 9971−9981

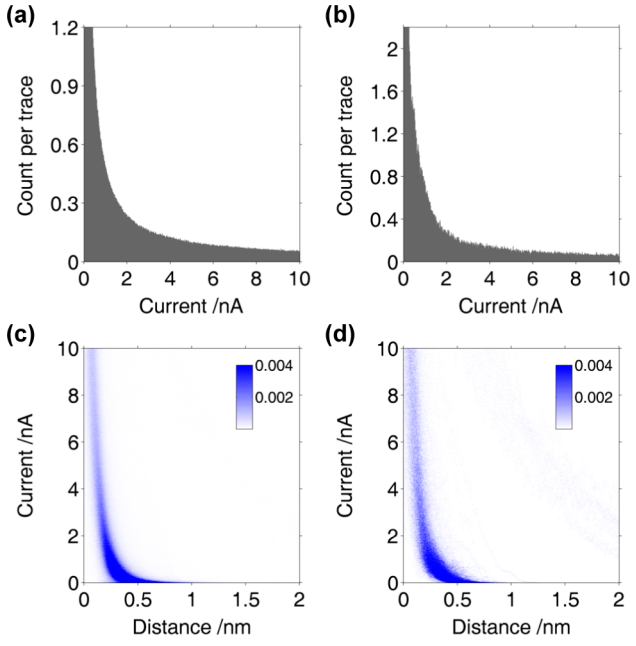

Figure 6. Top: Normalized 1D (a) all data point (10 000 traces) and (b) algorithm-selected (872 traces) current-count histograms for the **blank** 10 000 series (V_{bias} = 0.3 V, I_0 = 20 nA; 0.012 nA/bin). Bottom: Normalized 2D (c) all data point and (d) algorithm-selected current-distance-count histograms from the same data set (0.01 nA × 0.002 nm/bin).

B, and high/C), our result corresponds to a single-molecule in the medium group configuration (suggested to be an all-*trans* conformation coupled to single Au atoms at one or both sides[4]). For the **blank** series, no current peaks or other features are visible despite the fact that 9% of traces were selected. A comparison between both 10 000 series indicates that many more long plateaus (selected using higher PDBCs) are present in the selected traces from the **1,8-ODT** series than those from the **blank** (Figure S13 and S14). Examples of selected $I(s)$ traces from the latter are given in the SI, Figure S23, showing also that the short "plateau" features occur at indeterminate current values. Accordingly, we attribute these characteristics to experimental noise.

To calculate the molecular junction length with **1,8-ODT** we first determined the initial tip−substrate distance (s_0 = 0.59 nm) using the method of Haiss et al. and eq 3 (see SI, Figure S24 and associated discussion).[5] In brief, this approach works by extrapolation of featureless exponential decay curves (measured from I_0 at s_0) back to the current which corresponds to formation of the metal−metal contact (assumed here as G_0, where s = 0 nm).[19] The average junction rupture/break-off distance (s_b) was next determined by finding the distance for each algorithm-selected trace (2859 traces) at which the measured current reached the noise level of our system (for more details see SI, Figure S25 caption). A histogram of these distances initially yielded a bimodal distribution, with peaks at ∼0.7 nm and ∼1 nm (SI, Figure S25b). Given that the sorting parameters used to select $I(s)$ traces for the **1,8-ODT** series also selected a number of traces in the **blank** series (PDBC ≥ 30), we hypothesized that the peak at ∼0.7 nm was attributable to the selected subset of featureless exponential $I(s)$ traces. It is notable that a well-defined single peak at s_b = 0.68 nm was also observed by performing an identical s_b analysis for selected traces of the **blank** 10 000 series (SI, Figure S25d; PDBC ≥ 30). Adjusting the sorting parameters so that they would select <1% of traces in the **blank** series (PDBC ≥ 50), we reran the s_b analysis, now with 686 fewer selected traces (2,173 total, featureless exponentials excluded). As a result the peak at ∼0.7 nm was significantly diminished, while the remaining peak appeared unchanged. This monomodal distribution was fitted to provide $s_{b(\mathbf{1,8\text{-}ODT})}$ = 0.93 nm (SI, Figure S25c). With the above approach, a total junction length ($s_t = s_0 + s_b$) of 1.52 nm was obtained, in very good agreement with the theoretical value for Au-**1,8-ODT**-Au (1.59 nm, estimated using ChemBio3D Ultra 12.0, CambridgeSoft/PerkinElmer).

$$S_0 = \frac{\ln\left(G_0 \cdot \frac{V_{bias}}{I_0}\right)}{-\mathrm{d}\ln(I)/\mathrm{d}s} \tag{3}$$

Smaller Data Sets: 2000 I(s) Traces/Experiment. While 10 000 $I(s)$ traces/experiment appears to provide sufficient data for robust statistical analysis, we were interested in exploring the quality of smaller data sets. Taking fewer measurements would improve our ability to more rapidly screen components under changing conditions (varying V_{bias}, I_0, etc.). We found 2000 traces per experiment was a convenient number, allowing us to run 10 experiments in just ∼22 h (with intermittent surface imaging).

Using our automated macro, we measured 2000 $I(s)$ traces at 10 different V_{bias}−I_0 combinations (2000 series, 20 000 $I(s)$ traces/set). Noting that s_0 decreases with decreasing V_{bias} at constant I_0 (and vice versa), we chose appropriate values of I_0 so as to keep s_0 constant (V_{bias} = ± 0.1 V, I_0 = 6.5 nA; V_{bias} = ± 0.2 V, I_0 = 13.5 nA; V_{bias} = ± 0.3 V, I_0 = 20 nA; V_{bias} = ± 0.4 V, I_0 = 26 nA; V_{bias} = ± 0.5 V, I_0 = 32.5 nA). These were calculated using eq 3, using experimental measurements of $\mathrm{d}\ln I/\mathrm{d}s$ from the **1,8-ODT** 10 000 series (SI, Figure S24 and S25). Experimentally determined values at all $V_{bias} - I_0$ combinations ultimately showed s_0 was indeed constant across all experiments (SI, Figure S26; mean = 0.57 ± 0.1 nm, error = 1 s.d.). Each 10 × 2000 traces set was conducted *in triplicate* for both **1,8-ODT** coated and **blank** Au substrates, using freshly electrochemically polished and annealed Au substrates and newly etched Au STM tips. After processing data sets using our selection algorithm (120 000 traces in total), on average we found $JFP_{(\mathbf{1,8\text{-}ODT})}$ = 47 ± 6% and $JFP_{(\mathbf{blank})}$ = 18 ± 5% (SI, Figure S26; error = 1 s.d. from the mean). Though there is some apparent correlation between JFP and V_{bias} or chronological order of experiment in our data (experiment order was randomized with respect to V_{bias}), we consider this a fortuitous result without real physical meaning. Furthermore, Grubbs' test for outliers determined no outliers in the mean or raw data sets (assuming the variation in JFP is normally distributed).

As previously observed for the **1,8-ODT** 10 000 series, algorithm-selected 1D current-count histograms each showed a single current peak (Figure 7a), albeit not necessarily as well-defined (Figure 5). Nonetheless a clear V_{bias} dependence was observed, with the most probable current value from each experiment again approximated by fits comprising a single Gaussian distribution. The mean values were plotted against V_{bias} (Figure 7b) where a linear fit of the data provided a conductance value of 4.02 nS (5.19×10^{-5} G_0, error = ± 0.10 nS *or* 0.13×10^{-5} G_0, least-squares estimate of the standard error). A linear I−V relationship at low bias has been observed previously for **1,8-ODT**,[20,58] and is in good agreement with the Simmons model for a rectangular tunneling barrier.[59,60] Values of $s_{t(\mathbf{1,8\text{-}ODT})}$ were obtained as described above (data selected

DOI: 10.1021/jacs.5b05693
J. Am. Chem. Soc. 2015, 137, 9971−9981

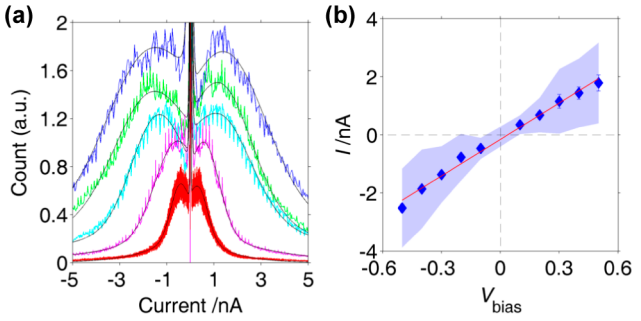

Figure 7. (a) Representative 1D current-count algorithm-selected histograms (2000 curves/experiment) taken from the same sample (1000 bins/histogram, counts scaled for clarity). Histograms range from $V_{bias} = \pm 0.1$ V (red plots), to $V_{bias} = \pm 0.5$ V (blue plots), where the black lines are fits comprising a single Gaussian. (b) A plot of most probable current against V_{bias} for **1,8-ODT** (2000 traces/experiment, series repeated *in triplicate*; histograms used for peak fitting comprised 1000 bins). The linear fit (red line) provides a conductance value of 4.02 nS. Error bars represent 1 s.d. from the mean of the most probable current values; shaded area represents the mean fwhm of the peak fits.

with PDBC ≥ 50). These were found to be independent of changing $V_{bias} - I_0$ combination, with the average (1.48 ± 0.02 nm, error = 1 s.d. from the mean) in good agreement with the result obtained for the 10 000 series (SI, Figure S27). As before, 1D and 2D histograms from the **blank** 2000 series exhibited no clear peaks or other significant features.

Testing Limits: 100 000 I(s) Traces/Experiment. Noting a small shoulder peak at ∼0.5 nA in the sorted 1D histogram of the **1,8-ODT** 10 000 series (Figure 5b), and additional variability across the 2000 series sets, it was of interest to determine if these apparent peaks were real features or the results of an incomplete statistical data set (where subsets of plateaus had not yet been fully averaged). Using the aforementioned methods, we now collected and analyzed 100 000 $I(s)$ traces of **1,8-ODT** on Au from the same sample over 3 days (100 000 series; $V_{bias} = 0.3$ V, $I_0 = 20$ nA). Figure 8

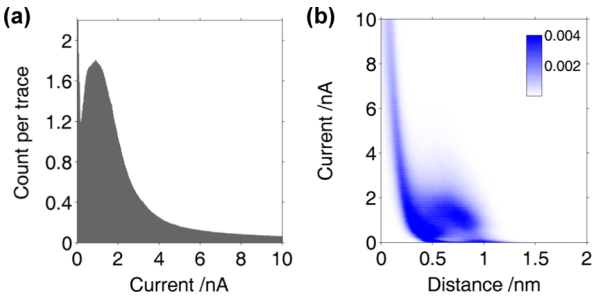

Figure 8. Normalized (a) 1D current-count (0.012 nA/bin) and (b) 2D current-distance-count algorithm-selected (45 240 traces) histograms for the **1,8-ODT** 100 000 series ($V_{bias} = 0.3$ V, $I_0 = 20$ nA (0.01 nA × 0.002 nm/bin).

shows 1D and 2D histograms prepared from algorithm-selected data. Again a perfect fit to the data using only a single Gaussian distribution was not possible, though this particular situation could be improved by using two Gaussians: one with a peak current close to the original (single Gaussian) value, the other at ∼2 times this value (SI, Figure S28). This may suggest that part of our fitting difficulties could be due to measurements of current through multiple molecules at a time. Furthermore, we cannot discount the possibility that we are sampling multiple conductance groups (noted briefly above). These are frequently observed with alkanedithiols, where changes in the nature of bonding between the Au-thiol linkages impacts the measured through-molecule current.[2−5,61−65] For comparison with previous series, fits comprising a single Gaussian suggest the most probable conductance to be 3.43 nS (4.43×10^{-5} G_0; with a HWHM based on Gaussian fitting = 3.35 nS *or* 4.33×10^{-5} G_0), with $s_t = 1.48$ nm.

To track any possible changes at the substrate over the 3 days of measurement, we also plotted 1D and 2D histograms for every 10 000 $I(s)$ traces of the same data set (SI, Figure S28). No obvious trends with most probable current, JFP, s_0, s_b or s_t were observed (SI, Figure S30 and S31). However, close inspection of the 10 × 10 000 trace 1D histograms reveal subtle changes in peak shape, width and fine structure, in line with the discussions above.

Plateau Frequency Analysis. Despite subtle variability between experiments, the broad consistency and reproducibility of our results leads us to question if we might be sampling a single conductance group predominately. It could be the case, for example, that our strict substrate cleaning protocols and regularly applied tip voltage pulses fashion and maintain electrode surfaces of a particularly consistent structure. Alternatively, particular surface bound molecules of **1,8-ODT** might be more susceptible to forming a molecular junction than others (perhaps residing in similar molecular environments).

Notable in this context, we occasionally observed experiments which provided a significantly lower JFP (<10%) than expected based on our previous studies. As both low and high JFP data sets were obtained across different Au substrates, **1,8-ODT** solutions (always 40 s immersion), and STM tips, we suggest that such variations result simply from adventitious sample or solution contamination. Unfortunately, at concentrations of ∼0.01 mM we were below the detection limits of available NMR, mass spectrometry and GC instruments, making it difficult to interrogate the solutions directly. No discernible differences could be established between stock solutions of higher concentration.

To provide additional insights into the homogeneity of our **1,8-ODT**-functionalized Au surfaces, we considered how JFP might vary as a function of tip position (Figure 9). If the substrate surface was homogeneous (**1,8-ODT** randomly distributed, spatially invariant probability toward junction

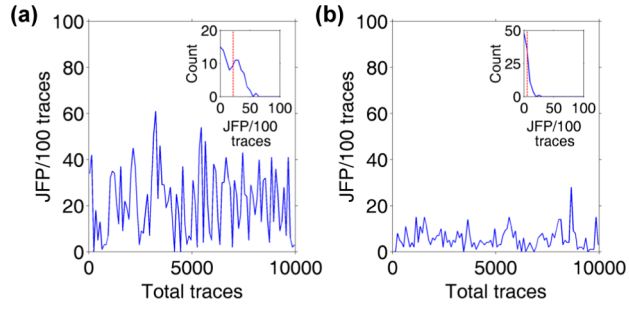

Figure 9. Variation of JFP with changing tip position (PDBC ≥ 50; 10 000 traces) when running $I(s)$ experiments on different Au substrates. These demonstrate either (a) high JFP (21.7%, the 10 000 series presented above; $V_{bias} = 0.3$ V, $I_0 = 20$ nA) or (b) low JFP (5.7%; $V_{bias} = 0.4$ V, $I_0 = 26$ nA). Inset: histograms showing the most probable values of JFP/100 traces (BW = 5, red dotted line represents mean JFP).

DOI: 10.1021/jacs.5b05693
J. Am. Chem. Soc. 2015, 137, 9971−9981

formation), we would expect the JFP (say per 100 traces), to be independent of tip position. Otherwise, one might expect to observe two or more populations in the JFP probability distribution, e.g., when some areas on the surface exhibit low JFP, while others show high JFP. Reasons for such behavior include an inhomogeneous distribution of molecules on the surface, temporary tip "contamination" or variations in the surface binding mode (e.g., when both thiol groups are bound to the substrate surface). The data shown in Figure 9 illustrates both scenarios, namely for experiments with high and low overall JFP (panels (a) and (b), respectively; plotted as average JFP/100 traces). The insets represent the corresponding histograms. In panel (a), two distinct statistical populations are observed, one monotoneously decaying at low JFP, a second one superimposed with a peak around JFP = 28. A similar result is observed for the 100 000 series (substrate functionalized with the same 0.01 mM solution), suggesting that the observed behavior is not due to incomplete statistical sampling (SI, Figure S32). On the other hand, the same analysis applied to the data shown in panel (b) shows low overall JFP and a single, roughly exponentially decaying JFP distribution. To support these arguments, using a MATLAB script we performed stochastic simulations of $I(s)$ experiments at different surface coverages (1 and 25%, respectively) and a random distribution of molecules on a surface with 100 by 100 binding sites. The tip was taken to be sufficiently sharp that only a single molecule can bind at any given time with a probability of 100% (in principle, the code also allows for blunt tips and thus "contact" to more than one molecule) and each simulation ran through 10 000 cycles (tip approaches); see SI for further details. In accordance with expectations and as shown in Figure S34, the JFP histograms resemble the two individual populations shown in Figure 9a, namely a monotoneously decaying JFP distribution at 1% surface coverage and a (roughly) normal-distributed JFP histogram for 25% surface coverage. Combining the two then yields the overall distribution observed experimentally (in panel (a)), even though the actual reason for the surface inhomogeneity is difficult to establish based on the $I(s)$ data alone.

For insights into the physical origin of these observations, we looked to other reports into self-assembled layers of alkanethiols on Au(111). Electrochemical capacitance measurements indicate that contact of a Au surface with a 0.01 mM **1,8-ODT** solution for 40 s (our immersion conditions) may actually result in around 50−60% surface coverage.[66,67] From STM imaging studies, it is also suggested that alkanethiols and alkanedithiols of various chain lengths can form low coverage (laying-flat) and high coverage (standing-up) phases on Au(111).[68−73] It is therefore possible that our observations could be explained by differences in local surface coverage at submonolayer loadings. Interestingly, this would also suggest that such molecular configurations do not appreciably change during the time scale of our experiments (at least, not during measurements at a given STM tip−surface position). Where the local surface concentration is low, molecules may be more likely to lie down and less likely to connect to a STM tip held ∼0.59 nm above the surface (providing low JFP tip positions). Where the local surface coverage is high, molecules may be more likely to stand up and connect to the STM tip more frequently (providing high JFP tip positions). Further investigations to improve our understanding of how surface orientation of molecules at submonolayer coverage affects JFP and other measurements of single-molecule properties are required.

"Plateaus" Exhibiting Distinct Shapes. From the 2D histograms plotted here it is notable that a large majority of the plateaus measured follow a distinct and unusual low-current to high-current feature (normally, only the opposite is found[4]). While the periodicity of this motif (∼0.34) suggests it might relate to the underlying electrode structure (Au−Au nearest neighbor spacing = 0.29 nm),[74,75] as discussed below this may not account for all observations.

Though rarely observed, similar characteristics have been identified in previous room temperature BJ studies of alkanes[10,76] and very recently organosilanes[77] (also in experiments at low temperature[78]). With alkanes [HS−$(CH_2)_x$−SH, x = 6, 8],[10,76] current increases have been attributed to changes from *gauche* to all-*trans* configurations upon stretching (with additional low to high current features apparently assigned to the stochastic connection of additional molecules in junctions during stretching).[77] With organosilanes [MeS−CH_2−$(SiH_2)_x$−CH_2−SMe, x = 2−10], this unusual plateau shape was instead attributed to an improved coupling between Au electrodes and the fully elongated molecule facilitated by stereoelectronic changes. Density functional theory (DFT) calculations supported the hypothesis that only those molecular conformations comprising terminal *ortho* dihedral geometries were able to facilitate a strong σ-conjugation through the S-Me anchor group and organosilane backbone. This effect was subsequently exploited for mechanical switching from high (low) to low (high) conductance states upon compression (elongation) of the junction. Interestingly, an alkane analogue [MeS−$(CH_2)_8$−SMe], with only poorly conjugated σ-bonds, exhibited the opposite effect−low (high) to high (low) conductance changes upon mechanical compression (elongation) of the junction. This was attributed to the expected changes in the through-space junction conductance component. However, it is intriguing that analogous features also predominate in current-distance measurements of *thiol*-terminated alkanes (this work and ref[10,76]). Hoft et al. have previously suggested a rationale for why increases in tunneling current upon junction elongation may be observed with chemisorbed (covalently bound), but not physisorbed, S−Au contacts.[79] Here they propose that decreasing hybridization between the S and Au based orbitals upon bond stretching ultimately leads to a large, narrow peak just below the Fermi level in the transmission spectrum at large S−Au distances (and so to a maximum in the tunneling current). Unfortunately, our STM setup does not yet permit analogous measurements of compression/elongation cycles to explore these effects in further detail.

While the low-to-high current plateau shape predominates in our experiments, numerous other motifs can be identified which occur less frequently (Figure 10). These intriguing patterns are not represented by the "most probable" picture provided by the 2D histograms, and pose several immediate questions. Are different shapes related to specific molecular starting conformations, and if so can they provide fresh insights into the local molecular structure on the surface, or the mechanics of pulling single-molecule junctions? Can their relative frequency be controlled, and so provide a handle to modulate junction conductance? By visual inspection, it is not obvious how many classes or groups there are, nor if they are distinct or form a continuum of states between each other (particularly given the added complication of experimental

DOI: 10.1021/jacs.5b05693
J. Am. Chem. Soc. 2015, 137, 9971−9981

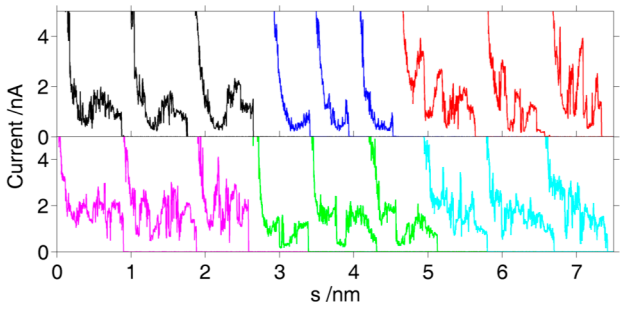

Figure 10. A variety of algorithm-selected, hand-grouped plateau shapes observed with **1,8-ODT** (taken from the 10 000 series, traces displaced along the *x*-axis for clarity). Top left: the only shape well-represented in 2D histograms.

noise). Counting by hand, the algorithm-sorted traces from the **1,8-ODT** 10 000 series (PDBC ≥ 30, 2859 traces) appear to contain ∼671 (23%) traces which look to be noisy, featureless exponentials. This is in excellent agreement with the number removed when sorting this data set using PDBC ≥ 50 (686 traces), an approach discussed previously. Of the remaining 2188 traces, around 755 (35%) traces comprise a "plateau" feature which approximates the shape represented in the 2D histograms (that of Figure 10, top left), leaving ∼1433 (65%) traces comprising "events" of other shapes. The development of objective mathematical tools to classify through-molecule conductance features based on their shape is highly desirable.

CONCLUSION

We have detailed a new methodology for automated single molecule conductance measurements using the $I(s)$ technique, which also combines intermittent STM imaging. Critical here was the development of an unsupervised data sorting algorithm (utilizing underlying tunneling characteristics, noise and event detection) which was used to objectively improve signal-to-noise ratios. Within the present work, up to 100 000 traces per experiment have been obtained. This allows for comprehensive and rigorous statistical analysis, as well as long-term stability studies of chemically modified surfaces at the single-molecule scale (an important criterion for real-world devices).

Application of our methodology to a model system, Au-**1,8-ODT**-Au, shows good reproducibility and single-molecule conductance values in excellent agreement with those observed elsewhere ($\sim 5 \times 10^{-5}$ G_0). Plateau frequency analysis reveals that the JFP is not normally distributed around the mean value in $I(s)$ experiments of **1,8-ODT** on Au(111). Instead, two distinct statistical populations result from "low JFP" and "high JFP" tip−substrate positions (a conclusion also supported by simulations). The apparent inhomogeneity of functionalized surfaces at submonolayer coverage suggests that local concentrations and/or the orientation of surface-bound molecules can have a significant impact on the mean JFP observed. We stress that such analyses are only possible using a combined all data point and objective data selection ("middle ground") methodology such as the one described herein. Finally−given our observations of several well-defined "plateau" shapes which are not apparent in 2D histograms−we highlight the need for additional tools to analyze subgroups within data sets. These may lead to an improved understanding of molecular junctions that cannot readily be drawn from statistical averages. This work showcases the potential of the $I(s)$ approach for investigating relatively unexplored yet exciting areas in single-molecule spectroscopy.

EXPERIMENTAL SECTION

Materials. 1,8-ODT (≥97%, Sigma-Aldrich) and absolute EtOH (VWR International) were used without further purification. Water was purified using a Purite Select Fusion system to a resistivity of 18.2 MΩ cm. Nitrogen (industrial grade, >99.998%) and hydrogen (research grade, >99.9995%) were from BOC (UK). Single-crystal Au substrates (orientation (111), 99.999% purity, polished with roughness <0.01 μm and orientation accuracy <0.1°) were from MaTecK GmbH (Juelich, Germany). Au (>99.99%, diameter = 0.25 mm) and Pt wire (>99.9%, diameter = 1 mm) was from Goodfellow.

Scanning Tunneling Microscopy (STM). *STM Tip Preparation.* Au wire was electrochemically etched in HCl/EtOH using a CHI760C potentiostat (CH Instruments, Austin, Texas) via the method of Wang et al.[80] After etching, tips were washed in EtOH and water and dried in air. Approximately 25% proved suitable for use in $I(s)$ experiments. Tips were ultimately rejected if they could not maintain a good tunneling contact with the substrate (for example, demonstrating poor overlap between topography trace/retrace scans during imaging). Such tips were typically unable to clearly resolve characteristic Au surface features, and recorded mostly noisy $I(s)$ traces.

Substrate Preparation. Prior to coating with analyte for $I(s)$ experiments, single-crystal Au substrates were cleaned by a rigorous electropolishing/annealing protocol. First they were supported on a Pt wire coil (anode) and immersed with a second Pt wire loop (cathode) in 0.1 M H_2SO_4. Application of 5.5 V DC for ∼15 min produced a red oxide layer which was subsequently removed by dissolution in 1 M HCl. This process was typically repeated *in triplicate*, whereby the substrate was thoroughly rinsed with water then furnace-annealed at 850 °C for 36 h (NaberTherm LE 4/11/R6). Immediately prior to use, the Au substrates were placed in an alumina boat (Z561754, Sigma-Aldrich) and heated repeatedly (≥3 times) in a hydrogen flame to bright orange (maintaining this color for 10−20 s) with ∼10 s cooling intervals. After 40 s immersion in analyte solutions (∼0.01 mM **1,8-ODT** in EtOH), Au substrates were thoroughly rinsed with EtOH and dried in a stream of nitrogen. These were fixed in position during STM experiments using a custom PTFE cell. The latter, as with all glassware used, was cleaned by first boiling in 20% nitric acid then sonicating for 10 min. All items were rinsed thoroughly with ultrapure water between steps, and oven-dried before use.

STM Setup. Imaging and $I(s)$ measurements were performed in air using an Agilent 5100 STM operated using PicoView 1.14 (Agilent Technologies). During $I(s)$ experiments PicoView was itself controlled using a macro, written with and played using Macro Scheduler (MJT Net Ltd., UK). A linear current STM scanner was used for all experiments (preamp sensitivity = 10 nA/V, bandwidth = 1.6 kHz).

Data Analysis. Sorting algorithms were written and tested using MATLAB release 2014a, The MathWorks, Inc., Natick, MA.[53] STM images were processed using WSxM 5.0 Develop 7.0, Nanotec Electrónica, S.L.[81]

ASSOCIATED CONTENT

Supporting Information

Additional experimental information, data and discussion, Macro Scheduler code for data collection, MATLAB script for data sorting and a representative data set (**1,8-ODT** 10 000 series). The Supporting Information is available free of charge on the ACS Publications website at DOI: 10.1021/jacs.5b05693. It is also available at http://zenodo.org (10.5281/zenodo.18051, 10.5281/zenodo.18048, 10.5281/zenodo.18050).

AUTHOR INFORMATION

Corresponding Authors

*michael.inkpen08@imperial.ac.uk

DOI: 10.1021/jacs.5b05693
J. Am. Chem. Soc. 2015, 137, 9971−9981

*n.long@imperial.ac.uk
*t.albrecht@imperial.ac.uk

Notes

The authors declare no competing financial interest.

■ ACKNOWLEDGMENTS

MSI, ML, NF, NJL and TA thank the Leverhulme Trust for funding (RPG 2012−754). RJN and DCM gratefully acknowledge the EPSRC for funding (EP/K007785/1).

■ REFERENCES

(1) Xu, B.; Tao, N. J. *Science* **2003**, *301*, 1221.
(2) Ulrich, J.; Esrail, D.; Pontius, W.; Venkataraman, L.; Millar, D.; Doerrer, L. H. *J. Phys. Chem. B* **2006**, *110*, 2462.
(3) Venkataraman, L.; Klare, J. E.; Tam, I. W.; Nuckolls, C.; Hybertsen, M. S.; Steigerwald, M. L. *Nano Lett.* **2006**, *6*, 458.
(4) Li, C.; Pobelov, I.; Wandlowski, T.; Bagrets, A.; Arnold, A.; Evers, F. *J. Am. Chem. Soc.* **2007**, *130*, 318.
(5) Haiss, W.; Martín, S.; Leary, E.; Zalinge, H. v.; Higgins, S. J.; Bouffier, L.; Nichols, R. J. *J. Phys. Chem. C* **2009**, *113*, 5823.
(6) *Nat. Nanotechnol.* **2013**, *8*, 377, DOI: 10.1038/nnano.2013.116.
(7) *Nat. Nanotechnol.* **2013**, *8*, 385, DOI: 10.1038/nnano.2013.101.
(8) Lortscher, E. *Nat. Nanotechnol.* **2013**, *8*, 381.
(9) Venkataraman, L.; Klare, J. E.; Nuckolls, C.; Hybertsen, M. S.; Steigerwald, M. L. *Nature* **2006**, *442*, 904.
(10) Fujihira, M.; Suzuki, M.; Fujii, S.; Nishikawa, A. *Phys. Chem. Chem. Phys.* **2006**, *8*, 3876.
(11) Jang, S.-Y.; Reddy, P.; Majumdar, A.; Segalman, R. A. *Nano Lett.* **2006**, *6*, 2362.
(12) Mishchenko, A.; Zotti, L. A.; Vonlanthen, D.; Bürkle, M.; Pauly, F.; Cuevas, J. C.; Mayor, M.; Wandlowski, T. *J. Am. Chem. Soc.* **2011**, *133*, 184.
(13) Haiss, W.; van Zalinge, H.; Higgins, S. J.; Bethell, D.; Höbenreich, H.; Schiffrin, D. J.; Nichols, R. J. *J. Am. Chem. Soc.* **2003**, *125*, 15294.
(14) Haiss, W.; Wang, C.; Grace, I.; Batsanov, A. S.; Schiffrin, D. J.; Higgins, S. J.; Bryce, M. R.; Lambert, C. J.; Nichols, R. J. *Nat. Mater.* **2006**, *5*, 995.
(15) Wang, C.; Batsanov, A. S.; Bryce, M. R.; Martín, S.; Nichols, R. J.; Higgins, S. J.; García-Suárez, V. M.; Lambert, C. J. *J. Am. Chem. Soc.* **2009**, *131*, 15647.
(16) Nichols, R. J.; Haiss, W.; Higgins, S. J.; Leary, E.; Martin, S.; Bethell, D. *Phys. Chem. Chem. Phys.* **2010**, *12*, 2801.
(17) He, J.; Sankey, O.; Lee, M.; Tao, N.; Li, X.; Lindsay, S. *Faraday Discuss.* **2006**, *131*, 145.
(18) Hihath, J.; Tao, N. *Nanotechnology* **2008**, *19*, 265204.
(19) Scullion, L.; Doneux, T.; Bouffier, L.; Fernig, D. G.; Higgins, S. J.; Bethell, D.; Nichols, R. J. *J. Phys. Chem. C* **2011**, *115*, 8361.
(20) Kay, N. J.; Nichols, R. J.; Higgins, S. J.; Haiss, W.; Sedghi, G.; Schwarzacher, W.; Mao, B.-W. *J. Phys. Chem. C* **2011**, *115*, 21402.
(21) Kay, N. J.; Higgins, S. J.; Jeppesen, J. O.; Leary, E.; Lycoops, J.; Ulstrup, J.; Nichols, R. J. *J. Am. Chem. Soc.* **2012**, *134*, 16817.
(22) Marques-Gonzalez, S.; Yufit, D. S.; Howard, J. A. K.; Martin, S.; Osorio, H. M.; Garcia-Suarez, V. M.; Nichols, R. J.; Higgins, S. J.; Cea, P.; Low, P. J. *Dalton Trans.* **2013**, *42*, 338.
(23) Bennett, N. Ph.D. Thesis, Cardiff University, December 2010.
(24) Haiss, W.; Wang, C.; Jitchati, R.; Grace, I.; Martín, S.; Batsanov, A. S.; Higgins, S. J.; Bryce, M. R.; Lambert, C. J.; Jensen, P. S.; Nichols, R. J. *J. Phys.: Condens. Matter* **2008**, *20*, 374119.
(25) Xia, J. L.; Diez-Perez, I.; Tao, N. J. *Nano Lett.* **2008**, *8*, 1960.
(26) Rascón-Ramos, H.; Artés, J. M.; Li, Y.; Hihath, J. *Nat. Mater.* **2015**, *14*, 517.
(27) Widawsky, J. R.; Kamenetska, M.; Klare, J.; Nuckolls, C.; Steigerwald, M. L.; Hybertsen, M. S.; Venkataraman, L. *Nanotechnology* **2009**, *20*, 434009.
(28) Leary, E.; González, M. T.; van der Pol, C.; Bryce, M. R.; Filippone, S.; Martín, N.; Rubio-Bollinger, G.; Agraït, N. s. *Nano Lett.* **2011**, *11*, 2236.
(29) Dulić, D.; Pump, F.; Campidelli, S.; Lavie, P.; Cuniberti, G.; Filoramo, A. *Angew. Chem., Int. Ed.* **2009**, *48*, 8273.
(30) González, M. T.; Wu, S.; Huber, R.; van der Molen, S. J.; Schönenberger, C.; Calame, M. *Nano Lett.* **2006**, *6*, 2238.
(31) Quek, S. Y.; Venkataraman, L.; Choi, H. J.; Louie, S. G.; Hybertsen, M. S.; Neaton, J. B. *Nano Lett.* **2007**, *7*, 3477.
(32) Reddy, P.; Jang, S.-Y.; Segalman, R. A.; Majumdar, A. *Science* **2007**, *315*, 1568.
(33) Widawsky, J. R.; Darancet, P.; Neaton, J. B.; Venkataraman, L. *Nano Lett.* **2011**, *12*, 354.
(34) Guo, S.; Zhou, G.; Tao, N. *Nano Lett.* **2013**, *13*, 4326.
(35) Widawsky, J. R.; Darancet, P.; Neaton, J. B.; Venkataraman, L. *Nano Lett.* **2012**, *12*, 354.
(36) Aviram, A.; Ratner, M. A. *Chem. Phys. Lett.* **1974**, *29*, 277.
(37) Elbing, M.; Ochs, R.; Koentopp, M.; Fischer, M.; Hänisch, C. v.; Weigend, F.; Evers, F.; Weber, H. B.; Mayor, M. *Proc. Natl. Acad. Sci. U. S. A.* **2005**, *102*, 8815.
(38) Batra, A.; Darancet, P.; Chen, Q.; Meisner, J. S.; Widawsky, J. R.; Neaton, J. B.; Nuckolls, C.; Venkataraman, L. *Nano Lett.* **2013**, *13*, 6233.
(39) Díez-Pérez, I.; Hihath, J.; Lee, Y.; Yu, L.; Adamska, L.; Kozhushner, M. A.; Oleynik, I. I.; Tao, N. J. *Nat. Chem.* **2009**, *1*, 635.
(40) Müri, M.; Gotsmann, B.; Leroux, Y.; Trouwborst, M.; Lörtscher, E.; Riel, H.; Mayor, M. *Adv. Funct. Mater.* **2011**, *21*, 3706.
(41) Castellanos-Gomez, A.; Bilan, S.; Zotti, L. A.; Arroyo, C. R.; Agraït, N.; Carlos Cuevas, J.; Rubio-Bollinger, G. *Appl. Phys. Lett.* **2011**, *99*, 123105.
(42) Kim, T.; Liu, Z.-F.; Lee, C.; Neaton, J. B.; Venkataraman, L. *Proc. Natl. Acad. Sci. U. S. A.* **2014**, *111*, 10928.
(43) Mamin, H. J.; Guethner, P. H.; Rugar, D. *Phys. Rev. Lett.* **1990**, *65*, 2418.
(44) Guo, C. X.; Thomson, D. J. *Ultramicroscopy* **1992**, *42*−*44*, 1452.
(45) Chang, C. S.; Su, W. B.; Tsong, T. T. *Phys. Rev. Lett.* **1994**, *72*, 574.
(46) Binnig, G.; Rohrer, H.; Gerber, C.; Weibel, E. *Appl. Phys. Lett.* **1982**, *40*, 178.
(47) Lee, T.; Wang, W.; Klemic, J. F.; Zhang, J. J.; Su, J.; Reed, M. A. *J. Phys. Chem. B* **2004**, *108*, 8742.
(48) Akkerman, H. B.; Boer, B. d. *J. Phys.: Condens. Matter* **2008**, *20*, 013001.
(49) von Wrochem, F.; Scholz, F.; Yasuda, A.; Wessels, J. M. *J. Phys. Chem. C* **2009**, *113*, 12395.
(50) Lange, K. L.; Little, R. J. A.; Taylor, J. M. G. *J. Am. Stat. Assoc.* **1989**, *84*, 881.
(51) Jones, M. C.; Faddy, M. J. *J. R. Stat. Soc.* **2003**, *65*, 159.
(52) Gelman, A.; Carlin, J. B.; Stern, H. S.; Dunson, D. B.; Vehtari, A.; Rubin, D. B. *Bayesian Data Analysis*, 3rd ed.; CRC Press: Boca Raton, FL, 2014.
(53) *MATLAB* release 2014a; The MathWorks, Inc.: Natick, MA, 2014.
(54) Li, X.; He, J.; Hihath, J.; Xu, B.; Lindsay, S. M.; Tao, N. *J. Am. Chem. Soc.* **2006**, *128*, 2135.
(55) Li, Z.; Pobelov, I.; Han, B.; Wandlowski, T.; Błaszczyk, A.; Mayor, M. *Nanotechnology* **2007**, *18*, 044018.
(56) Sek, S.; Misicka, A.; Swiatek, K.; Maicka, E. *J. Phys. Chem. B* **2006**, *110*, 19671.
(57) Wierzbinski, E.; Slowinski, K. *Langmuir* **2006**, *22*, 5205.
(58) Cui, X. D.; Primak, A.; Zarate, X.; Tomfohr, J.; Sankey, O. F.; Moore, A. L.; Moore, T. A.; Gust, D.; Harris, G.; Lindsay, S. M. *Science* **2001**, *294*, 571.
(59) Simmons, J. G. *J. Appl. Phys.* **1963**, *34*, 1793.
(60) Cuevas, J. C.; Scheer, E. *Molecular Electronics: An Introduction to Theory and Experiment*; World Scientific Publishing Company: London, 2010.
(61) Sen, A.; Kaun, C.-C. *ACS Nano* **2010**, *4*, 6404.
(62) Hakkinen, H. *Nat. Chem.* **2012**, *4*, 443.

DOI: 10.1021/jacs.5b05693
J. Am. Chem. Soc. 2015, 137, 9971−9981

(63) Paz, S. A.; Michoff, M. E. Z.; Negre, C. F. A.; Olmos-Asar, J. A.; Mariscal, M. M.; Sanchez, C. G.; Leiva, E. P. M. *Phys. Chem. Chem. Phys.* **2013**, *15*, 1526.
(64) Kristensen, I. S.; Mowbray, D. J.; Thygesen, K. S.; Jacobsen, K. W. *J. Phys.: Condens. Matter* **2008**, *20*, 374101.
(65) Müller, K. H. *Phys. Rev. B: Condens. Matter Mater. Phys.* **2006**, *73*, 045403.
(66) Sur, U. K.; Subramanian, R.; Lakshminarayanan, V. *J. Colloid Interface Sci.* **2003**, *266*, 175.
(67) He, H.; Guo, Y.; Wang, S.; Jiang, Y. *Surf. Rev. Lett.* **2010**, *17*, 397.
(68) Poirier, G. E.; Pylant, E. D. *Science* **1996**, *272*, 1145.
(69) Kobayashi, K.; Yamada, H.; Horiuchi, T.; Matsushige, K. *Jpn. J. Appl. Phys.* **1998**, *37*, 6183.
(70) Darling, S. B.; Rosenbaum, A. W.; Wang, Y.; Sibener, S. J. *Langmuir* **2002**, *18*, 7462.
(71) Esplandiu, M. J.; Carot, M. L.; Cometto, F. P.; Macagno, V. A.; Patrito, E. M. *Surf. Sci.* **2006**, *600*, 155.
(72) Millone, M. A. D.; Hamoudi, H.; Rodríguez, L.; Rubert, A.; Benítez, G. A.; Vela, M. E.; Salvarezza, R. C.; Gayone, J. E.; Sánchez, E. A.; Grizzi, O.; Dablemont, C.; Esaulov, V. A. *Langmuir* **2009**, *25*, 12945.
(73) Vericat, C.; Vela, M. E.; Benitez, G.; Carro, P.; Salvarezza, R. C. *Chem. Soc. Rev.* **2010**, *39*, 1805.
(74) Yanson, A. I.; Bollinger, G. R.; van den Brom, H. E.; Agraït, N.; van Ruitenbeek, J. M. *Nature* **1998**, *395*, 783.
(75) Cheng, Z. L.; Skouta, R.; Vazquez, H.; Widawsky, J. R.; Schneebeli, S.; Chen, W.; Hybertsen, M. S.; Breslow, R.; Venkataraman, L. *Nat. Nanotechnol.* **2011**, *6*, 353.
(76) Suzuki, M.; Fujii, S.; Fujihira, M. *Jpn. J. Appl. Phys.* **2006**, *45*, 2041.
(77) Su, T. A.; Li, H.; Steigerwald, M. L.; Venkataraman, L.; Nuckolls, C. *Nat. Chem.* **2015**, *7*, 215.
(78) Temirov, R.; Lassise, A.; Anders, F. B.; Tautz, F. S. *Nanotechnology* **2008**, *19*, 065401.
(79) Hoft, R. C.; Ford, M. J.; Cortie, M. B. *Chem. Phys. Lett.* **2006**, *429*, 503.
(80) Wang, X.; Liu, Z.; Zhuang, M.-D.; Zhang, H.-M.; Wang, X.; Xie, Z.-X.; Wu, D.-Y.; Ren, B.; Tian, Z.-Q. *Appl. Phys. Lett.* **2007**, *91*, 101105.
(81) Horcas, I.; Fernández, R.; Gómez-Rodríguez, J. M.; Colchero, J.; Gómez-Herrero, J.; Baro, A. M. *Rev. Sci. Instrum.* **2007**, *78*, 013705.

DOI: 10.1021/jacs.5b05693
J. Am. Chem. Soc. 2015, 137, 9971−9981